

Energy backflow in unidirectional spatiotemporally localized wavepackets

Ioannis Besieris¹ and Peeter Saari^{2,3}

¹*The Bradley Department of Electrical and Computer Engineering,
Virginia Polytechnic Institute and State University, Blacksburg, Virginia 24060, USA*

²*Institute of Physics, University of Tartu, W. Ostwaldi 1, 50411, Tartu, Estonia and*

³*Estonian Academy of Sciences, Kohtu 6, 10130 Tallinn, Estonia**

(Dated: March 15, 2023)

Backflow, or retro-propagation, is a counterintuitive phenomenon where for a forward-propagating wave the energy locally propagates backward. In this study the energy backflow has been examined in connection with relatively simple causal unidirectional finite-energy solutions of the wave equation which are derived from a factorization of the so-called basic splash mode. Specific results are given for the energy backflow arising in known azimuthally symmetric unidirectional wavepackets, as well as in novel azimuthally asymmetric extensions. Using the Bateman-Whittaker technique, a novel finite-energy unidirectional null localized wave has been constructed that is devoid of energy backflow and has some of the topological properties of the basic Hopfion.

PACS numbers: 03.50.De, 41.20.Jb, 42.25Bs, 42.25.Fx

I. INTRODUCTION

In general terms, the phenomenon of backflow takes place when some quantity (probability or energy density flow, local momentum, etc.) in some spatio-temporal region of a wavefield is directed backward with respect to the directions of all plane-wave constituents of the wavefield [1, 2]. Position probability backflow specific to quantum particles, such as electrons, has been termed ‘quantum backflow,’ and this subject is actively studied (see the newest review [3] and references therein). A dispute arose recently over the distinction between the quantum backflow and backflow phenomena known in classical field theories [2, 4]. In our opinion, the contradistinction here is largely of a terminological nature. At least nobody doubts that backflow is a wave phenomenon that may occur in all kinds of wavefields, particularly in those describable by the Schrödinger or the Maxwell or the wave equations in free space.

Indeed, already a simple field of four appropriately polarized and directed electromagnetic plane waves exhibit prominent energy backflow described by the Poynting vector whose direction is reversed with respect to the direction of propagation of the resultant wave [5–7]. In the physical optics community the energy backflow in sharply focused light has been known more than an half a century and has been thoroughly studied theoretically recently [8–10]. In the context of quantum backflow, monochromatic optical fields have been used for recent experimental verification of the effect [11, 12]. Energy backflow in electromagnetic Bessel beams has been analytically demonstrated in [13, 14]. In the context of our present subject, important is the theoretical study [15] of backflow in pulsed electromagnetic X waves, which belong to the class of the so-called localized waves.

Localized waves (LWs)—also known as space-time wavepackets (STWP)—have been studied intensively during the past thirty years (see [16–30] for pertinent literature). They constitute spatiotemporally localized solutions to various hyperbolic equations governing acoustic, electromagnetic and quantum wave phenomena and can be classified according to their group velocity as luminal LWs, or focus wave modes (FWM), superluminal LWs, or X waves (XWs), and subluminal LWs. Further details can be found in two edited monographs on the subject [31, 32] and in the recent thorough review article [33]. In general, both linear and nonlinear LW pulses exhibit distinct advantages in comparison to conventional quasi-monochromatic signals. Their spatiotemporal confinement and extended field depths render them especially useful in diverse physical applications. Experimental demonstrations have been performed in the acoustical and optical regimes [20, 22, 25, 34–38]. Work, however, has been carried out at microwave frequencies recently [39–41].

An important question—widely discussed especially in the early stages of the theoretical study of LWs at the end of the last century—has been the physical realizability of localized waves. For example, two- or three-dimensional electromagnetic luminal localized waves in free space involve the characteristic variables $\varsigma = z - ct$ and $\eta = z + ct$ of the one-dimensional scalar wave equation. Consequently, they contain both forward and backward propagating components. Tweaking free parameters appearing in the wavepackets can significantly reduce the backward components. However, it is principally crucial whether the plane-wave constituents of the wavepacket propagate only in the positive z -direction or also backward. In the first case not only the wave can be launched from an aperture as a freely propagating beam but, also, the very question of energy backflow is meaningful.

In the literature, the LWs with forward-propagating plane-wave constituents have been called somewhat mis-

* Corresponding author: peeter.saari@ut.ee

leadingly 'causal'. In the following discussion we shall use the term 'unidirectional'. It must be pointed out, however, that, in general, a wavepacket as a whole can propagate in the positive z -direction despite the fact that its plane-wave constituents are omnidirectional; and *vice versa*: the group velocity of a packet may have a negative z -component despite the fact that the z -components of the wavevectors of all its plane-wave constituents are positive. Also, for LWs the group velocity typically differs from the energy velocity, see [42, 43].

Our aim in this article is to theoretically study several representatives of a class of causal, purely unidirectional *finite-energy* localized waves with particular emphasis on their energy backflow characteristics. Specifically, we shall try to ascertain the role of the vector nature and polarization properties of a light field in the emergence of the backflow effect and its strength. The paper is organized as follows. In the next section we consider several finite-energy unidirectional localized waves

known from the literature. Extended unidirectional LWs will be introduced in Sec. 3. Sec. 4 is devoted to a detailed analysis of the backflow characteristics of a unidirectional vectorial LW derived from the so-called splash mode solution of the scalar wave equation. This LW is a generalization of the unidirectional solution used by Bialynicki-Birula *et al.* [2] to demonstrate the existence of the backflow in electromagnetic fields. Section 5 is devoted to the derivation of a finite-energy Hopfion-like spatiotemporally localized wave that is devoid of energy backflow. Concluding remarks are made in Sec. 6.

II. CAUSAL, SCALAR UNIDIRECTIONAL LOCALIZED WAVES

The feasibility of a finite-energy, causal, unidirectional localized wave was first addressed by Lekner [44] using the Fourier synthesis

$$\begin{aligned}\psi_+(\rho, z, t) &= \int_0^\infty dk_z e^{ik_z z} \int_0^\infty dk e^{-ikct} \int_0^\infty d\kappa \kappa J_0(\kappa\rho) \delta(-\kappa^2 - k_z^2 + k^2) F(\kappa, k_z, k) \\ &= \int_0^\infty dk e^{-ikct} \int_0^k dk_z e^{ik_z z} \sqrt{k^2 - k_z^2} J_0\left(\rho\sqrt{k^2 - k_z^2}\right) F_1(k_z, k).\end{aligned}\quad (1)$$

Choosing the spectrum

$$F_1(k_z, k) = \frac{k_z e^{-ka}}{\sqrt{k^2 - k_z^2}}, \quad a > 0, \quad (2)$$

one obtains

$$\begin{aligned}\psi_+(\rho, z, t) &= \\ &= \int_0^\infty dk e^{-k(a+ict)} \int_0^k dk_z k_z e^{ik_z z} J_0\left(\rho\sqrt{k^2 - k_z^2}\right).\end{aligned}\quad (3)$$

Carrying out the integrations, Lekner has derived the causal unidirectional solution

$$\begin{aligned}\psi_+(\rho, z, t) &= \\ &= \frac{a^4 \hat{a}^3 (\hat{a}^2 + \rho^2)^2 - 6z^2 (\hat{a}^2 + \rho^2) - z^4 + 8iz (\hat{a}^2 + \rho^2)^{3/2}}{3 (\hat{a}^2 + \rho^2)^{3/2} (\hat{a}^2 + \rho^2 + z^2)^3},\end{aligned}\quad (4)$$

with $\tilde{a} = a + ict$. By interchanging the order of integrations in Eq. (3) and using table integrals from [45], p. 191, No. 10 and p. 133, No. 3, we obtained a more compact expression for the same unidirectional solution:

$$\psi(\rho, z, t) = \frac{a^4 \hat{a} \left(3\sqrt{\rho^2 + \hat{a}^2} - iz\right)}{3(\rho^2 + \hat{a}^2)^{3/2} \left(\sqrt{\rho^2 + \hat{a}^2} - iz\right)^3}.\quad (5)$$

A formal study of a causal, unidirectional localized wave was undertaken by So, Plachenov and Kiselev [46] starting from the finite-energy luminal splash mode [18, 19]

$$\psi(\rho, z, t) = \frac{1}{[a_1 + i(z - ct)][a_2 - i(z + ct)] + \rho^2}, \quad (6)$$

where $a_{1,2}$ are positive free parameters. As mentioned in the introduction, this is a bidirectional solution. However, for $a_2 \gg a_1$, the backward components are significantly reduced. So *et al.* [46] decomposed the denominator in Eq. (6) as follows:

$$\begin{aligned}\psi(\rho, z, t) &= \\ &= \frac{1}{z_*^2 - S^2} = \frac{1}{S} \left(\frac{1}{z_* - S} - \frac{1}{z_* + S} \right) = \frac{1}{2} (u_+ - u_-); \\ &\quad S = \sqrt{ct_*^2 - \rho^2}; \\ &\quad t_* = t + \frac{i(a_2 + a_1)}{2c}, \quad z_* = z + \frac{i(a_2 - a_1)}{2}.\end{aligned}\quad (7)$$

They proved that the expression $u_+ = S^{-1}(z_* - S)^{-1}$ satisfies the wave equation and is solution propagating in the positive z -direction. On the other hand, u_- is a solution propagating purely in the negative z -direction. They did not analyze whether u_+ is unidirectional (causal) in the sense we use here, that all its plane-wave constituents propagate solely into the hemisphere with $k_z > 0$.

Independently, Bialynicki-Birula *et al.* [2] introduced two luminal unidirectional wavepackets

$$h_{\pm} = \frac{1}{2} \frac{1}{\sqrt{c^2(a+it)^2 + \rho^2}} \frac{1}{\sqrt{c^2(a+it)^2 + \rho^2 \mp iz}}, \quad (8)$$

where $a > 0$, which they derived by a Fourier syn-

$$h_{\pm}(\rho, z, t) = \frac{1}{2} \int_{-\infty}^{\infty} dk_z H(\pm k_z) e^{ik_z z} \int_0^{\infty} d\kappa \kappa J_0(\kappa \rho) e^{-ict \sqrt{\kappa^2 + k_z^2}} G(\kappa, k_z), \quad (9)$$

where $H(\cdot)$ designates the Heaviside unit step function which ensures the integration in one hemisphere only. Choosing the spectrum

$$G(\kappa, k_z) = \frac{1}{\sqrt{\kappa^2 + k_z^2}} e^{-ac\sqrt{\kappa^2 + k_z^2}}, \quad a > 0 \quad (10)$$

and introducing the new variable $\lambda = \sqrt{\kappa^2 + k_z^2}$, one obtains

$$h_{\pm}(\rho, z, t) = \frac{1}{2} \int_{-\infty}^{\infty} dk_z H(\pm k_z) e^{ik_z z} \int_{k_z}^{\infty} d\lambda J_0(\rho \sqrt{\lambda^2 - k_z^2}) e^{-a\lambda}. \quad (11)$$

The integration over λ is carried out [45], p. 191, No. 9, yielding

$$h_{\pm}(\rho, z, t) = \frac{1}{2\sqrt{c^2(a+ict)^2 + \rho^2}} \times \int_{-\infty}^{\infty} dk_z H(\pm k_z) e^{ik_z z - |k_z| \sqrt{c^2(a+ict)^2 + \rho^2}}. \quad (12)$$

Finally, the integration over k_z results in the unidirectional solutions given in Eq. (8), where z is replaced by z_* , while the restriction $|\text{Im } z_*| < a$ avoids singularity. Note that the wavefunctions h_{\pm} given in Eq. (8), but modified in this manner, are equivalent, respectively, to $u_+/2$ and $u_-/2$ in Eq. (7), provided that, in addition, $a = (a_1 + a_2)/2$.

Without detailed discussion of its unidirectional features, a seemingly different type of solution was derived by Wong and Kaminer in 2017 [47]; specifically,

$$\psi(\rho, z, t) = -i \frac{a+ict}{k_0 \tilde{R}^2} \left(\frac{1}{k_0 \tilde{R}} f^{-s-1} + \frac{s+1}{s} f^{-s-2} \right); \quad (13)$$

$$f = 1 - k_0 \left(iz + a - \tilde{R} \right) / s, \quad \tilde{R} = \sqrt{(a+ict)^2 + \rho^2},$$

where $k_0 = \omega_0/c = 2\pi/\lambda_0$. This solution can be derived from the Fourier synthesis in Eq. (1). Assuming, first,

thesis and limiting the integration in k -space to one of the hemispheres (with $k_z > 0$ or $k_z < 0$, respectively). Here, we carry out the synthesis in a slightly modified version that incorporates complex values $z_* = z + iz_s$, $z_s \equiv (a_2 - a_1)/2$ of the z -coordinate and, thus, a two-parameter solution like in Eq. (7). Since the solution is axially symmetric, we base the synthesis on the zeroth-order Bessel beams; specifically,

the spectrum $F_1(k_z, k) = F_2(k_z) \exp(-ak)$, we obtain

$$\psi_+^1(\rho, z, t) = \frac{1}{\tilde{R}} \int_0^{\infty} dk_z e^{ik_z z} e^{-k_z \tilde{R}} F_2(k_z). \quad (14)$$

Let, next, $k_z/k_0 = \chi/s$ and choose the spectrum so that

$$\psi_+^1(\rho, z, t) = \frac{1}{\tilde{R}} \int_0^{\infty} d\chi e^{-\chi q} \frac{\chi^s}{\Gamma(s+1)}; \quad (15)$$

$$q = 1 - \frac{k_0}{s} \left(iz + a - \tilde{R} \right).$$

The final solution assumes the form

$$\psi_+^1(\rho, z, t) = \frac{1}{\tilde{R}} \left[1 - k_0 \left(iz + a - \tilde{R} \right) \right]^{-s-1} = \frac{1}{\tilde{R}} f^{-s-1}. \quad (16)$$

The solution given in Eq. (13) results from differentiation of $\psi_+^1(\rho, z, t)/k_0$ with respect to time.

All the unidirectional wavepackets discussed in this section are finite-energy solutions of the three-dimensional scalar wave equation in free space. An important question is how do they propagate in the positive z -direction? We shall answer this question in connection to the Bialynicki-Birula *et al.* [2] wavepacket which seems to be the simplest. Consider the part of the solution involving z and t ; specifically,

$$z = -i \sqrt{c^2(a+it)^2 + \rho^2}. \quad (17)$$

Then, the real group speed is given by

$$v_g(\rho, t) = \text{Re} \left\{ \frac{\partial}{\partial t} z(\rho, t) \right\} = c \text{Re} \left\{ \frac{c(a+it)}{\sqrt{c^2(a+it)^2 + \rho^2}} \right\}. \quad (18)$$

It is seen that the group speed depends both on the radial distance and time. A plot of the group speed (normalized with respect to the speed of light in vacuum equal to unity) is shown in Fig. 1 for three values of ρ . On axis ($\rho = 0$), $v_g = 1$ for all values of time. At $\rho = 2$, the speed is subluminal (but very close to unity) for small values of time, it becomes luminal at a value of time slightly larger than 10, superluminal afterwards, and tends to unity for

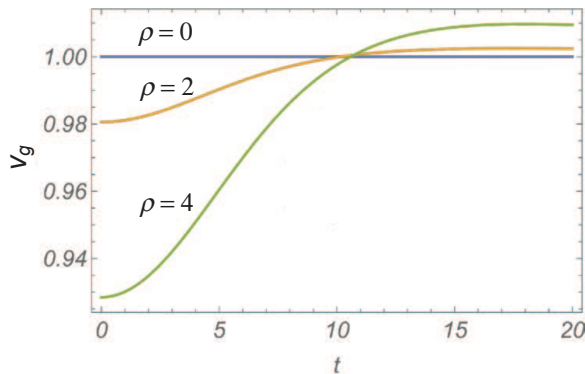


FIG. 1. Plot of the normalized ($c = 1$) group speed vs. time for $\rho = 0, 2, 4$ and parameter value $a = 10$. Here and in the subsequent figures the parameters, coordinates, and time are given in dimensionless length units, see also the paragraph after Eq. (26).

very large values of time. A similar behavior is exhibited for larger values of ρ .

This behavior is different from a finite-energy unidirectional scalar wavepacket moving at a fixed speed. An example is provided in Appendix A for a solution to the equation of acoustic pressure under conditions of uniform flow.

III. EXTENDED SCALAR UNIDIRECTIONAL LOCALIZED WAVES

Courant and Hilbert [48] have pointed out that a "relatively undistorted" progressive solution to the homogeneous three-dimensional (3D) scalar wave equation in vacuum assumes the form

$$\psi(\vec{r}, t) = \frac{1}{g(\vec{r}, t)} f[\theta(\vec{r}, t)], \quad (19)$$

where $f(\cdot)$ is essentially an arbitrary function, $\theta(\vec{r}, t)$, referred to as the "phase" function, is a solution to the nonlinear characteristic equation

$$\left(\frac{\partial\theta}{\partial x}\right)^2 + \left(\frac{\partial\theta}{\partial y}\right)^2 + \left(\frac{\partial\theta}{\partial z}\right)^2 - \frac{1}{c^2}\left(\frac{\partial\theta}{\partial t}\right)^2 = 0, \quad (20)$$

and $g(\vec{r}, t)$ is an "attenuation" function; the latter depends on the choice of $\theta(\vec{r}, t)$, but not in a unique manner. Along this vein, a very general class of solutions to the homogeneous scalar wave equation in free space is given as

$$\begin{aligned} \psi_+(\vec{r}, t) &= \frac{1}{g(\vec{r}, t)} f[\theta(\alpha, \beta)]; \\ g(\vec{r}, t) &\equiv \sqrt{\rho^2 - c^2(t - it_s)^2}, \\ \alpha(\vec{r}, t) &\equiv \sqrt{\rho^2 - c^2(t - it_s)^2} - i(z + iz_s), \\ \beta(\vec{r}, t) &\equiv \frac{\rho e^{-i\phi}}{ic(t - it_s) + g(\vec{r}, t)}, \end{aligned} \quad (21)$$

in polar coordinates. Here, z_s and t_s are free positive parameters. In the sequel, we shall discuss in detail the specific azimuthally asymmetric solution

$$\psi_+(\rho, \phi, z, t) = \frac{1}{2g(\vec{r}, t)} \frac{1}{\alpha^q(\vec{r}, t)} e^{-p\alpha(\vec{r}, t)} \beta^m(\vec{r}, t), \quad (22)$$

where p is a positive free parameter. It should be noted that for $m = 0$, $p = 0$ and $q = 1$, the solution $\psi_+(\vec{r}, t)$ is identical to the Bialynicki-Birula azimuthally symmetric expression h_+ given in Eq. (8) if $z_s = 0$ and $t_s = a$. Also, for $m = 0$, $p = 0$ and $q = s + 1$, $\psi_+(\vec{r}, t)$ is a slight variation of the expression $\psi_+^1(\rho, z, t)$ in Eq. (16).

IV. ENERGY BACKFLOW IN UNIDIRECTIONAL SPATIOTEMPORAL LOCALIZED WAVES

A. Scalar-valued wave theory

The energy transport equation corresponding to the (3+1)D homogeneous scalar wave equation

$$\left(\nabla^2 - \frac{1}{c^2} \frac{\partial^2}{\partial t^2}\right) \psi(\vec{r}, t) = 0 \quad (23)$$

governing the *real-valued* wave function $\psi(\vec{r}, t)$ in free space is given as [49, 50]

$$\nabla \cdot \vec{S} + \frac{\partial}{\partial t} U = 0, \quad (24)$$

where

$$U = \frac{1}{2} \frac{1}{c^2} \left(\frac{\partial}{\partial t} \psi\right)^2 + \frac{1}{2} \nabla \psi \cdot \nabla \psi \quad (25)$$

is the energy density (J/m^3) and

$$\vec{S} = -\frac{\partial}{\partial t} \psi \nabla \psi \quad (26)$$

is the energy flow density vector (W/m^2).

An examination of energy backflow is accomplished by examining the properties of the z -component of the energy flow vector corresponding to the real part of the extended unidirectional scalar complex wave function $\psi_+(\rho, \phi, z, t)$ given in Eq. (22). Plots are shown in Fig. 2 of S_z versus ρ for four axial positions, first for $m = 0$, $p = 0$, $q = 1$ and then, in Fig. 2(b) for $m = 3$, $p = 0$, $q = 1$. For both plots the parameter values are $t_s = 0.3$ and $z_s = 0.1$. The time is fixed at $t = 0.5$, with the speed of light of vacuum normalized to unity. Thus, the parameters and time are given in dimensionless length units and therefore the results are applicable not only in optical but also in microwave, etc. regions. For example, if the chosen values of the parameters t_s and z_s , as well as the time t were in micrometers, then $t = 0.5$ would correspond to 1.67 femtoseconds which would also

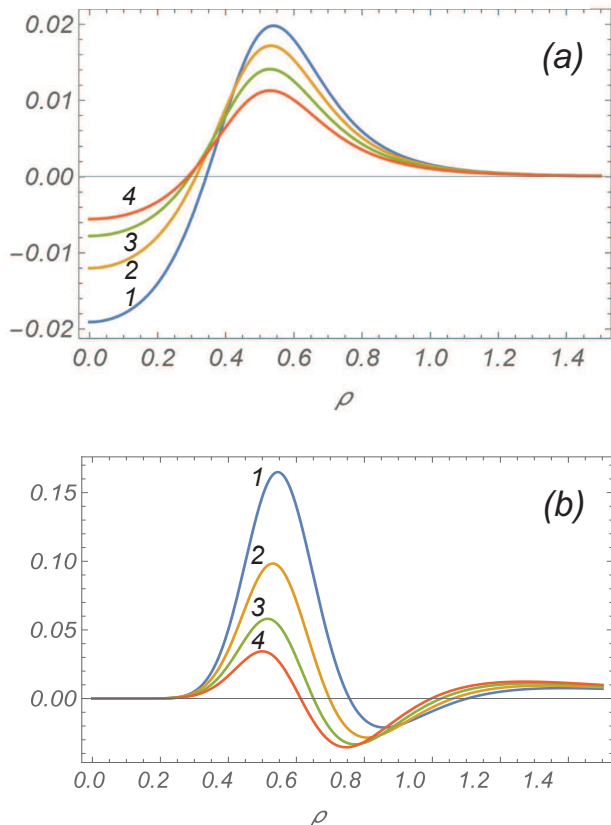


FIG. 2. Plots of the longitudinal component of the energy flow vector S_z at $t = 0.5$, with the speed of light normalized to unity. (a) $m = 0$, $q = 1$, $p = 0$. (b) $m = 3$, $q = 1$, $p = 0$. For curves 1, 2, 3, 4, values of the axial coordinate are $z = 0.9$, $z = 1.0$, $z = 1.1$, and $z = 1.2$, respectively. The plots are normalized with respect to their peak intensities at $t = 0$.

be approximately equal to the pulsewidth. The value $t = 0.5$ has been chosen since at $t = 0$ the backflow is absent but at higher values of t the pulse would spread out too much and the energy flow would become negligible.

We studied the simplest case with $m = 0$, $p = 0$, $q = 1$ in more detail by plotting the local energy transport velocity vector field, $\vec{V} = \vec{S}/U$, see Fig. 3. The plots demonstrate that at the instant $t = 0.5$ energy flows backward in the region ($\rho < 0.3, z > 0.5$). In a sense the situation resembles the sea drawback phenomenon, where the water recedes ahead of the tsunami wave peak.

A complex-valued version of the wavefunction of Eq. (22) exhibits practically no backflow effect because for its imaginary part the backflow regions have different locations as compared to those of the real part. Therefore, negative values of S_z from the real part are compensated by much stronger positive values of S_z from the imaginary part and *vice versa* since the energy flow vectors from both parts sum up additively. The same holds for the wavefunction of Eq. (5) or Eq. (4).

An interesting question is whether the power flux, that is the integral of the z -component of the energy flow

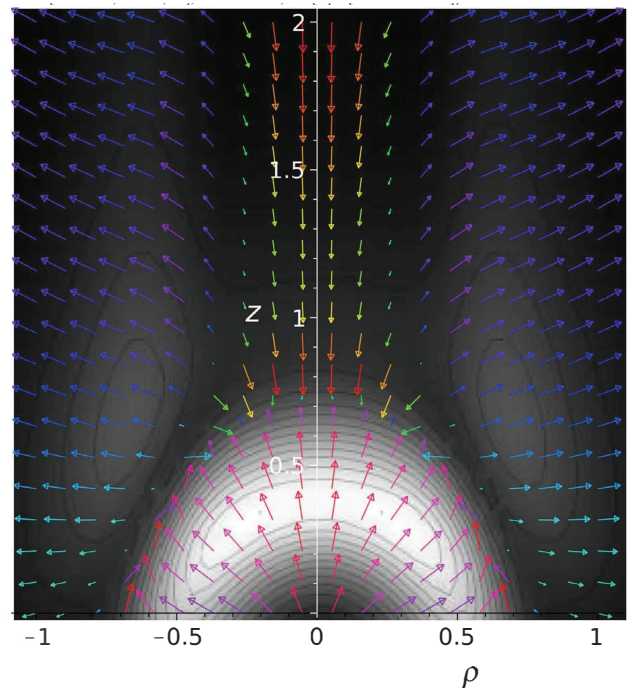


FIG. 3. Energy flow velocity vector field $\vec{V}(\rho, z)$ as the ratio of the energy flow vector \vec{S} and energy density U , plotted at 20×20 spatial points in the plane (x, z) , where $x = \pm \rho$ represents any transverse axis. The background image is a grey-scale plot (with contour lines) of \sqrt{U} and shows the pulse and its two weaker side-maxima at the instant $t = 0.5$ of their stage of evolution. The maximum length of arrows corresponds to c (or to 1 of the dimensionless velocity). In addition to the orientation of the arrows, values of the projection V_z are expressed by colors of the arrows in the on-line version: the color gamut violet-indigo-blue-cyan-green-yellow-red corresponds to range from $+1$ to -1 (cyan corresponds to 0). Other parameters are the same as in Fig. 2(a).

vector over a transverse plane at fixed values of z and t can be negative, at least for a small circular disk. Indeed, this is the case. From Fig. 2(a), we use the dimensionless values $z = 0.9$ and $t = 0.5$. Then, the integration results in the plot are shown in Fig. 4.

We see that the negative flux increases in absolute value up to the radius $\simeq 0.26$ of the disk, in full accordance with Fig. 3.

To conclude, it is somewhat surprising that a scalar solution to the wave equation exhibits the backflow effect because earlier studies have instilled an opinion that the effect appears in electromagnetic fields of specific polarization. Our results indicate that backflow is possible not only in optical fields describable by scalar approximation but also in acoustical fields.

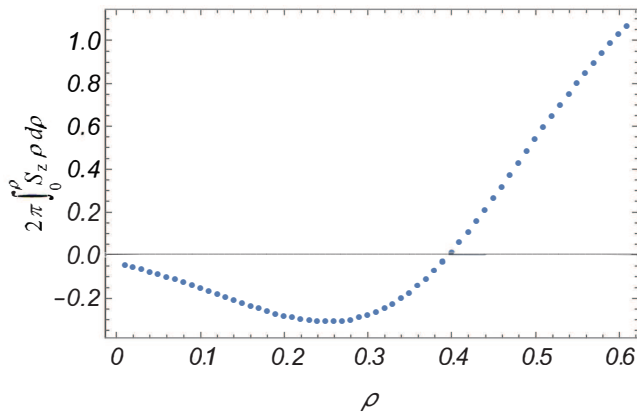


FIG. 4. Plot of the numerical evaluation of the power through a circular disk, with values of the radial coordinate in the range $\{0, 0.6\}$ in intervals of $1/100$ at the fixed values $z = 0.9$ and $t = 0.5$, with the speed of light normalized to unity. The plot corresponds to that in Fig. 2(a) for $m = 0$, $p = 0$, $q = 1$ and the parameter values $t_s = 0.3$ and $z_s = 0.1$.

B. Vector-valued wave theory

Implicit in the article by Bialynicki-Birula *et al.* [2] is that the examination of the energy backflow characteristics of a vector-valued unidirectional localized wave is based on a complex Riemann-Silberstein vector [51, 52] derived from the vector Hertz potential $\vec{\Pi} = 2(\vec{a}_x + i\vec{a}_y)\psi$ in Cartesian coordinates, or $\vec{\Pi} = \exp(i\phi)(\vec{a}_\rho + i\vec{a}_\phi)\psi$ in cylindrical coordinates, where the complex-valued wave function $\psi(\vec{r}, t)$ is a solution of the (3+1)D scalar wave equation in free space; specifically, the function h_+ in Eq. (8). The complex-valued Riemann-Silberstein vector is defined as

$$\vec{F} = \nabla \times \nabla \times \vec{\Pi} + \frac{i}{c} \frac{\partial}{\partial t} \nabla \times \vec{\Pi}. \quad (27)$$

It obeys the equations

$$\nabla \times \vec{F} - \frac{i}{c} \frac{\partial}{\partial t} \vec{F} = 0, \quad \nabla \cdot \vec{F} = 0, \quad (28)$$

that are exactly equivalent to the homogeneous Maxwell equations for the free-space real electric and magnetic fields \vec{E} and \vec{B} , defined in terms of \vec{F} as follows:

$$\vec{F} = \sqrt{\frac{\varepsilon_0}{2}} (\vec{E} + ic\vec{B}). \quad (29)$$

The importance of the specific choice for the vector Hertz potential is that the corresponding Riemann-Silberstein vector, with the scalar wave function $\psi(\vec{r}, t)$ being *any luminal spatiotemporally localized wave* [e.g., the splash mode in Eq. (6)], is null, that is, it has the property $\vec{F} \cdot \vec{F} = 0$. Equivalently, the two Lorentz-invariant quantities $I_1 = \vec{E} \cdot \vec{B}$ and $I_2 = |\vec{E}|^2 - c^2|\vec{B}|^2$ are both equal to zero. Under certain restrictions, the resultant field

can be a pure Hopfion [53] exhibiting interesting topological properties, such as linked and knotted field lines, or a Hopfion-like structure, such as the one established by Bialynicki-Birula *et al.* [2].

In the discussion below, the formalism described above will be followed, however based on the simpler vector Hertz potential $\vec{\Pi} = \psi\vec{a}_z$. The Poynting vector, defined in terms of the real fields as $\vec{S} = \vec{E} \times \vec{H}$, can be written in terms of the Riemann-Silberstein vector and its complex conjugate as follows: $\vec{S} = -i\vec{F}^* \times \vec{F}$. An examination of energy backflow will be accomplished by examining the properties of the z -component of the Poynting vector corresponding to the extended unidirectional scalar complex wave function $\psi_+(\rho, \phi, z, t)$ given in Eq. (22). Plots are shown in Fig. 5 of S_z versus ρ for three axial

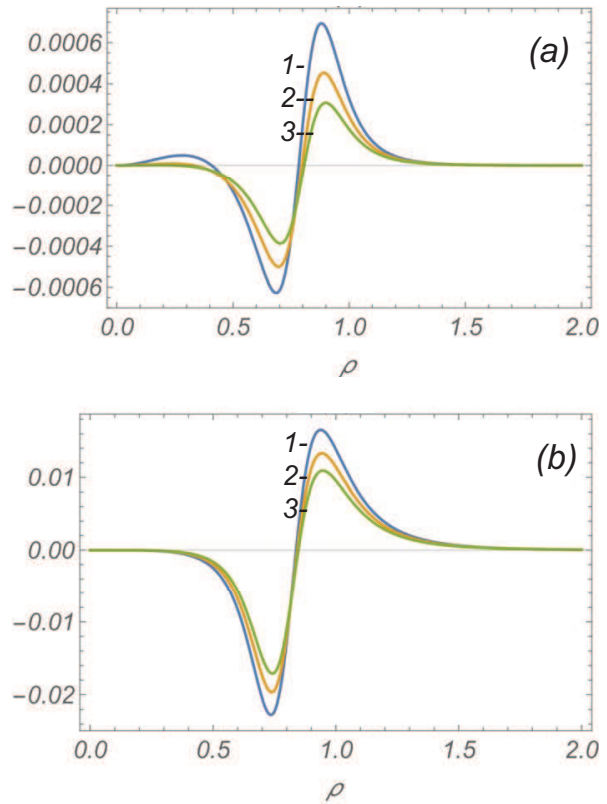


FIG. 5. Plots of the longitudinal component of the Poynting vector S_z at $t = 0.8$, with the speed of light normalized to unity. (a) $m = 0$, $p = 0$, $q = 1$. (b) $m = 3$, $p = 0$, $q = 1$. For curves 1, 2, 3, values of the axial coordinate are $z = 1.2$, $z = 1.3$, and $z = 1.4$ respectively. For both plots the parameter values are $t_s = 0.2$ and $z_s = 0.1$. Both plots are normalized with respect to their peak intensities at $t = 0$.

positions, first for $m = 0$, $p = 0$, $q = 1$ and then for $m = 3$, $p = 0$, $q = 1$. Note that the values of t and z , as well as of the parameters t_s and z_s differ from those of Fig. 2. We see that the vector-valued versions of both waves in a certain spatiotemporal region exhibit the backflow effect which is weak but comparable to that of the scalar-valued waves.

V. UNIDIRECTIONAL HOPFION-LIKE SPATIOTEMPORALLY LOCALIZED WAVE WITHOUT ENERGY BACKFLOW

The basic (or pure) Hopfion [53] is a finite-energy luminal spatiotemporally localized solution to Maxwell's equations in free space with unique topological properties. Specifically, all electric and magnetic field lines are closed loops, and any two electric (or magnetic) field lines are linked once with one another. However, the basic Hopfion has equally distributed forward (along the positive z -direction) and backward components. By construction, then, it exhibits energy backflow. The unidirectional Hopfion-like wave structure in [2] shares some of the topological characteristics with the pure Hopfion but exhibits energy backflow. A unidirectional Hopfion-

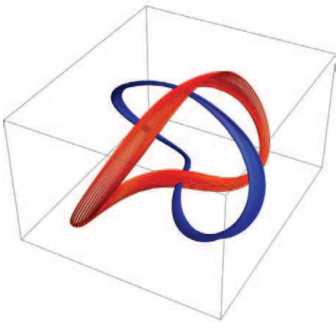


FIG. 6. Linkages of electric and magnetic field lines at a fixed value of time, with the speed of light in vacuum normalized to unity. The parameter values are $t_s = 0.3$ and $z_s = 0.1$.

like wave packet devoid of energy backflow will be con-

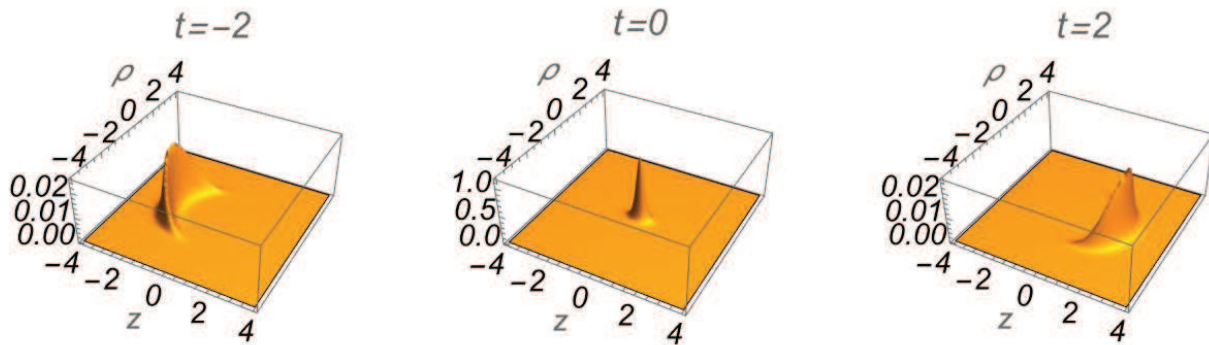


FIG. 7. Plot of the z -component of the Poynting vector versus z and ρ for three values of time, t . The parameter values are $t_s = 0.3$ and $z_s = 0.1$.

The ratio of the Poynting vector and the electromagnetic volume density is the local energy transport velocity

structured in this section. Toward this goal, a technique due originally to Whittaker [54] and Bateman [55] (see, also, [56, 57] for modern applications) will be used. First, the following two quantities, $\bar{\alpha}(\vec{r}, t)$ and $\bar{\beta}(\vec{r}, t)$, known as *Bateman conjugate functions*, will be defined in terms of the functions $\alpha(\vec{r}, t)$ and $\beta(\vec{r}, t)$ in Eq. (21):

$$\bar{\alpha}(\vec{r}, t) = \frac{1}{\alpha^{*2}(\vec{r}, t)}, \quad \bar{\beta}(\vec{r}, t) = \beta^*(\vec{r}, t). \quad (30)$$

Any functional of these two functions obeys the nonlinear characteristic Eq. (20). Furthermore, these two functions obey the *Bateman constraint*

$$\nabla \bar{\alpha} \times \nabla \bar{\beta} - \frac{i}{c} \left(\frac{\partial \bar{\alpha}}{\partial t} \nabla \bar{\beta} - \frac{\partial \bar{\beta}}{\partial t} \nabla \bar{\alpha} \right) = 0. \quad (31)$$

Under these assumptions, the complex vector

$$\vec{F} = \nabla \bar{\alpha} \times \nabla \bar{\beta} \quad (32)$$

is a *null Riemann-Silberstein vector* governed by the expressions in Eq. (28) and related to the real electric and magnetic fields as given in Eq. (29). These fields have some of the topological characteristics of those associated with a pure Hopfion. Fig. 6 shows the linkages of the electric and magnetic field lines. Similar linkages characterize any two electric (or magnetic) field lines. The basic Hopfion is characterized by linked single closed field line loops. In our case, we have linked bundles of field lines instead.

The z -component of the Poynting vector $\vec{S} = -i\vec{F}^* \times \vec{F}$ is plotted in Fig. 7. No energy backflow is present in this case.

$\vec{V}(\vec{r}, t) = \vec{S}/U$, with the energy density given in terms of the Riemann-Silberstein vector as $U(\vec{r}, t) = \vec{F}^* \cdot \vec{F}$.

Due to the nullity of \vec{F} , the modulus of the energy transport velocity is equal to the speed of light c , although $\vec{V}(\vec{r}, t)$ may vary in space and time. In the case of the basic Hopfion, the local energy velocity depends on the z and t through the combination $z - ct$; that is, it evolves along the z -direction without any deformation. Such a structure is known as a Robinson congruence. In the case under consideration in this section the local energy transport velocity is altogether independent of the coordinate z . The plot in Fig. 8 shows the z -component of the local energy transport velocity versus ρ for three values of time. The absence of energy backflow is clearly evident.

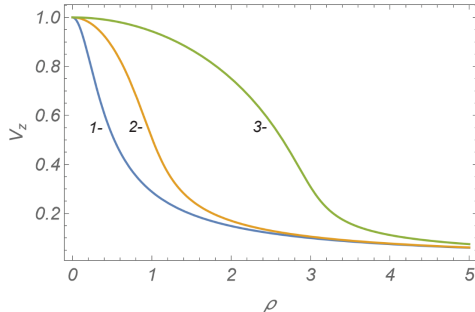


FIG. 8. Plot of the z -component of the local energy transport velocity versus ρ for three values of time, $t = 0.1, 1$ and $t = 3$.

VI. CONCLUDING REMARKS

As already has been mentioned, it is crucial whether the plane-wave constituents of a localized wavepacket propagate only in the positive z -direction or, also, backward. In the first case, not only the wave can be launched from an aperture as a freely propagating beam but, also, the very question of energy backflow is meaningful. Since most of the analytically constructed finite-energy spatiotemporally localized waves (luminal, subluminal, and superluminal) are acausal in the sense that they include both forward and backward propagating components, several attempts have been made to create close replicas of such waves that can be causally launched as forward beams from apertures (see, e.g., [21] and [58]), or even derive exact causal unidirectional wavepackets [59, 60]. Based usually on the Huygens principle, dealing with the former is computationally intensive. On the other hand, the latter are quite complicated analytically. The study of energy backflow in this article has been confined to relatively simple causal unidirectional finite-energy localized waves arising from a factorization of the basic splash mode [18, 19]. Specific results are given for the energy backflow exhibited in known azimuthally symmetric unidirectional wavepackets, as well as in novel azimuthally asymmetric extensions. Using the Bateman-Whittaker technique, a novel finite-energy unidirectional null localized wave has been constructed that is devoid of energy

backflow and has some of the topological properties of the basic Hopfion.

The study of energy backflow of the vector-valued unidirectional localized study in Sec. 4 was based on the Riemann-Silberstein complex vector that results in electric and magnetic fields that both have nonzero z components (non-TE and non-TM). Although specific results have not been incorporated in this article, an examination of the Poynting vectors associated individually with pure TE and TM fields associated to the scalar unidirectional localized wave $\psi_+(\rho, \phi, z, t)$ given in Eq. (22) shows the presence of energy backflow. This is altogether different from the cases of the superposition of four plane waves [5–7], Bessel beams [13, 14], and a pulsed electromagnetic X wave [15], all of which require a superposition of TE and TM fields for the appearance of energy backflow.

Finally, some remarks about possible experimental studies and relation of our results to quantum optics.

As was said already in Section III, the results (incl. numerical plots) are applicable irrespectively of the frequency range of the EM field. At low frequencies up to the microwave region, the measurements for studying the non-stationary behavior of Poynting vector in pulsed fields considered here require time resolution up to nanosecond range. For that purpose, known sensor-based techniques developed for monochromatic fields (see, e.g., [61]) would be applicable. However, to the best of our knowledge, no experiments have been carried out for electromagnetic or acoustic energy backflow associated with pulsed spatiotemporally localized wavefunctions.

As far as experiments on the electromagnetic energy backflow effect in the optical range is concerned, to date a few studies with monochromatic fields can be found: in addition to Refs. 11 and 12, studies of the effect in nanoscale focuses [62, 63] are appropriate to mention here. Distribution of the Poynting vector in optical fields can be measured via the motion of probe Rayleigh particles or via investigation of polarization in passage through an anisotropic crystal [64]. However, optical experiments on the fields considered in our paper are hardly feasible today because they would need near-single-cycle light pulses and—consequently—sub-femtosecond temporal resolution.

The expressions derived in this paper also apply to quantum optics: as it is known, the spatio-temporal dependence of the (quantum mechanical) wave function of a single photon, treated as a particle-like object, is given by the Riemann-Silberstein vector of the corresponding classical EM field. Moreover, as shown in [64], in terms of quantum weak measurements, observation of averaged trajectories of single photons can be considered as measurement of the distribution of the Poynting vector in the corresponding classical optical field, incl. backflow effects.

VII. APPENDIX A

The equation of acoustic pressure under conditions of uniform flow is given as follows:

$$\left[\nabla^2 - \frac{1}{u_0^2} \left(\frac{\partial}{\partial t} + \vec{u} \cdot \nabla \right)^2 \right] p(\vec{r}, t) = 0. \quad (\text{A1})$$

Here, u_0 is the speed of sound in the rest frame of the medium and \vec{u} is the uniform velocity of the background flow. In the special case where $\vec{u} = u\vec{a}_z$ and $u = u_0$ the resulting equation for the acoustic pressure simplifies as

follows:

$$\left(\nabla_t^2 - \frac{2}{u_0} \frac{\partial^2}{\partial t \partial z} - \frac{1}{u_0^2} \frac{\partial^2}{\partial t^2} \right) p(\vec{r}, t) = 0. \quad (\text{A2})$$

Under this assumption, several exact analytical infinite-energy nondiffracting and finite-energy slowly nondiffracting spatiotemporally localized wave solutions are supported. One such solution is the finite-energy unidirectional splash-like mode

$$p(\rho, z, t) = \frac{1}{a_1 + i(z - 2u_0 t)} \left(a_2 - iz + \frac{\rho^2}{a_1 + i(z - 2u_0 t)} \right)^{-q}, \quad (\text{A3})$$

with $a_{1,2}$ positive parameters. This is a finite-energy unidirectional wavepacket moving along the z -direction at the fixed speed $v = 2u_0$.

-
- [1] M. V. Berry, Quantum backflow, negative kinetic energy, and optical retro-propagation, *J. Phys. A: Math. Theor.* **43**, 415302 (2010).
- [2] I. Bialynicki-Birula, Z. Bialynicki-Birula and S. Augustynowicz, Backflow in relativistic wave equations, *J. Phys. Math. Gen.* **55**, 255702 (2022)
- [3] A. J. Bracken, Probability flow for a free particle: new quantum effects, *Phys. Scr.* **96**, 045201 (2021).
- [4] M. Barbier, C. J. Fewster, A. Goussev, G. Morozov, S. C. L. Srivastava, Comment on "Backflow in relativistic wave equations", arXiv:2210.05368 [quant-ph] 11 October 2022.
- [5] B. Z. Katsenelenbaum, What is the direction of the Poynting vector? *J. Commun., Technol. Electron.*, **42**, 119 (1997).
- [6] X.-L. You, C.-F. Li, Dependence of Poynting vector on state of polarization, arXiv:2009.04119 [physics.optics] 5 Jan 2021.
- [7] P. Saari and I. Besieris, Backward energy flow in simple four-wave electromagnetic fields, *Eur. J. Phys.* **42**, 055301 (2021).
- [8] B. Richards and E. Wolf, Electromagnetic diffraction in optical systems, II. Structure of the image field in an aplanatic system, *Proc. R. Soc. A* **253** 358 (1959).
- [9] V. V. Kotlyar, S. S. Stafeev, A. G. Nalimov, A. A. Kovalev, and A. P. Porfirev, Mechanism of formation of an inverse energy flow in a sharp focus, *Phys. Rev. A*, **101**, 033811 (2020).
- [10] H. Li, C. Wang, M. Tang, and A. Xinzhong, Controlled negative energy flow in the focus of a radial polarized optical beam, *Opt. Express* **28** 18607 (2020).
- [11] Y. Eliezer, T. Zacharias, and A. Bahabad, Observation of optical backflow, *Optica* **7**, 72 (2020).
- [12] A. Daniel, B. Ghosh, B. Gorzkowski, and R. Lapkiewicz, Demonstrating backflow in classical two beams' interference, arXiv:2206.05242 [physics.optics] 10 June 2022.
- [13] J. Turunen, A. T. Friberg, Self-imaging and propagation-invariance in electromagnetic fields, *Pure Appl. Opt.* **2**, 51 (1993).
- [14] A. V. Novitsky, D. V. Novitsky, Negative propagation of vector Bessel beams, *J. Opt. Soc. Am. A*, **24** 2844 (2007).
- [15] M. A. Salem and H. Bağcı, Energy flow characteristics of vector X-Waves, *Opt. Express* **19**, 8526 (2011).
- [16] J. N. Brittingham, Focus wave modes in homogeneous Maxwell equations: Transverse electric mode, *J. Appl. Phys.* **54**, 1179-1189 (1983).
- [17] A. P. Kiselev Modulated Gaussian beams, *Radio Phys. Quant. Electron.* **26**, 1014-1020 (1983).
- [18] R. W. Ziolkowski, Localized transmission of electromagnetic energy, *Phys. Rev. A* **39**, 2005-2033 (1989).
- [19] I. M. Besieris, A. M. Shaarawi and R. W. Ziolkowski, A bidirectional traveling plane wave representation of exact solutions of the scalar wave equation, *J. Math. Phys.* **30**, 1254-1269 (1989).
- [20] J. Y. Lu and J. F. Greenleaf, Nondiffracting X waves-exact solutions to the free space scalar wave equation and their finite aperture realization, *IEEE Trans. Ultrason. Ferroelectr. Freq. Contr.* **39**, 19-31 (1992).
- [21] R. W. Ziolkowski, I. M. Besieris and A. M. Shaarawi, Aperture realizations of the exact solutions to homogeneous-wave equations, *J. Opt. Soc. Am. A* **10**, 75-87 (1993).
- [22] P. Saari and K. Reivelt, Evidence of X-haped propagation-invariant localized light waves, *Phys. Rev. Lett.* **79**, 4135-4137 (1997).
- [23] I. M. Besieris, M. Abdel-Rahman, A. M. Shaaraw and A. Chatzipetros, Two fundamental representations of localized pulse solutions to the scalar wave equation, *Progr. Electromagn. Res. (PIER)* **19**, 1-48 (1998).
- [24] J. Salo, J. Fagerholm, A. T. Friberg and M. M. Saloma, Unified description of X and Y waves, *Phys. Rev. E* **62**, 4261 (2000).
- [25] R. Grunwald, V. Kebbel, U. Neumann, A. Kummrow, M. Rini, R. T. Nibbering, M. Piche, G. Rousseau and M. Fortin, Generation and characterization of spatially and temporally localized few-cycle optical wave packets,

- Phys. Rev. A **67**, 063820-1-5 (2003).
- [26] P. Saari and K. Reivelt, Generation and classification of localized waves by Lorentz transformations in Fourier space, Phys. Rev. E **69**, 036612-1-12 (2004).
- [27] S. Longhi, Spatial-temporal Gauss-Laguerre waves in dispersive media, Phys. Rev. E **68**, 066612 1-6 (2003).
- [28] C. Conti, S. Trillo, P. di Trapani, G. Valiulis, A. Piskarskas, O. Jedrkiewicz, and J. Trull, Nonlinear electromagnetic X waves, Phys. Rev. Lett. **90**, 170406 1-4 (2003).
- [29] A. P. Kiselev, Localized light waves: Paraxial and exact solutions of the wave equation (review), Opt. Spectrosc. **102**, 603-622 (2007).
- [30] M. Yessemov, B. Bhaduri, H. E. Kondaksi and A. F. Abouraddy, Classification of propagation-invariant space-time wavepackets in free spac: Theory and experiments, Phys. Rev. A **99**, 023856 (2019).
- [31] *Localized Waves*, edited by H. E. Hernandez-Figueroa, M. Zamboni-Rached, and E. Recami (J. Wiley, New York, 2007).
- [32] *Non-Diffracting Waves*, edited by H. E. Hernandez-Figueroa, E. Recami, and M. Zamboni-Rached (J. Wiley, New York, 2013).
- [33] M. Yessemov, L. A. Hall, K. L. Schepler and A. F. Abouraddy, Space-time wavepackets, Advances in Optics and Photonics **14**, 455-570 (2022).
- [34] K. Reivelt and P. Saari, Experimental demonstration of realizability of optical focus wave modes, Phys. Rev. E **66**, 056611-1-9 (2002).
- [35] P. Bownan, H. Valtna-Lukner, M. Löhmus, P. Piskars, P. Saari, and R. Trebino, Measurement of the spatio-temporal field of ultrashort Bessel-X pulses, Opt. Lett. **34**, 2276 (2009).
- [36] P. Saari, X-Type Waves in Ultrafast Optics, in [32] pp. 109-134.
- [37] H. F. Kondakci and A. F. Abouraddy, Diffraction-free space-time light sheets, Nat. Photon. **11**, 733-740 (2017).
- [38] B. Bhaduri, M. Yessemov, and A. F. Abouraddy, Space-time wave packets that travel in optical materials at the speed of light in vacuum, Optica **6**, 139-145 (2019).
- [39] N. Papisimakis, T. Raybould, V. A. Fedotov, D. P. Tsai, I. Youngs and N. I. Zheludev, Pulse generation scheme for flying electromagnetic doughnuts, Phys. Rev. B **97**, 201409-1-6 (2018).
- [40] D. Comite, W. Fuscaldo, S. K. Podilchak, and V. Gómez-Guillamón Buenndia, Microwave generation of X-waves by means of planar leaky-wave antenna, Appl. Phys. Lett. **113**, 144102-1-5 (2018).
- [41] W. Fuscaldo, D. Comite, A. Boesso, P. Baccarelli, P. Bughignoli and A. Galli, Focusing leaky waves: a class of electromagnetic localized waves with complex spectra, Phys. Rev. Appl. **9**, 054005-1-15 (2018).
- [42] P. Saari, Reexamination of group velocities of structured light pulses, Phys. Rev. A, **97**, 063824 (2018).
- [43] P. Saari, O. Rebane, and I. Besieris, Energy-flow velocities of nondiffracting localized waves, Phys. Rev. A **100**, 013849 (2019).
- [44] J. Lekner, Electromagnetic pulses, localized and causal, Proc. R. Soc. A **474**, 20170655 (2018).
- [45] *Tables of integral transforms*, edited by A. Erdelyi (McGraw-Hill, New York, 1954), Vol. I.
- [46] I. A. So, A. B. Plachenov and A. P. Kiselev, Simple unidirectional finite-energy pulses, Phys. Rev. A **102**, 063529 (2020).
- [47] L. J. Wong and I. Kaminer, Abruptly focusing and defocusing needles of light and closed-form electromagnetic wavepackets, ACS Photonics **4**, 1131 (2017).
- [48] R. Courant and D. Hilbert, *Methods of Mathematical Physics* (Interscience, New York, 1962), Vol. II.
- [49] H. S. Green and E. Wolf, A scalar representation of electromagnetic fields, Proc. Phys. Soc. A **66**, 1129 (1953).
- [50] L. Mandel and E. Wolf, *Optical Coherence and Quantum Optics* (Cambridge University Press, Cambridge, UK, 1995), p. 288.
- [51] H. Weber, *Die partiellen Differential-Gleichungen der mathematischen Physik nach Riemann's Vorlesungen*, Friedrich Vieweg und Sohn, Braunschweig, 1901.
- [52] L. Silberstein, Electromagnetische Grundgleichungen in bivectorieller Behandlung, Ann D. Phys. **22**, 579-686 (1907).
- [53] A. Ranāda, Knotted solutions of the Maxwell equations in vacuum, J. Phys. A: Math. Gen. **23**, L815-L820 (1990).
- [54] E. T. Whittaker, On the expressions of the electromagnetic field due to electrons by means of two scalar potential functions, Proc. London Math. Soc. **1**, 367-372 (1904).
- [55] H. Bateman, *The Mathematical Analysis of Electrical and Optical Wave-Motion on the Basis of Maxwell's Equations* (Dover, New York, 1955).
- [56] I. M. Besieris and A. M. Shaarawi, Hopf-Ranāda linked and knotted light beam solution viewed as a null electromagnetic field, Opt. Lett. **34**, 3887-3889 (2009).
- [57] H. Kedia, I. Bialynicki-Birula, D. Peralta-Salas and W. T. M. Irvine, Tying knots in light fields, Phys. Rev. Lett. **111**, 150404 (2017).
- [58] A. M. Shaarawi, Comparison of two localized wave fields generated from dynamic apertures, J. Opt. Soc. Am. A **14**, 1804-1815 (1997).
- [59] C. J. R. Sheppard and P. Saari, Lommel pulses: An analytic form for localized waves of the focus wave mode type with bandlimited spectrum, Opt. Express **16**, 150-160 (2008).
- [60] M. Zamboni-Rached, Unidirectional decomposition method for obtaining exact localized solutions totally free of backward components, Phys. Rev. A **79**, 013816 (2009).
- [61] C. C. Chen and J. F. Whitaker, An optically-interrogated microwave-Poynting vector sensor using cadmium manganese telluride. Opt. Express **18**, 12239 (2010).
- [62] G. Yuan, E. F. Rogers and N. I. Zheludev, "Plasmonics" in free space: observation of giant wavevectors, vortices, and energy backflow in superoscillatory optical fields, Light: Sci. Appl. **8**, 1 (2019).
- [63] V. V. Kotlyar, S. S. Stafeef, A. G. Nalimov, A. A. Kovalev and A. P. Porfirev, Experimental investigation of the energy backflow in the tight focal spot, Comp. Opt. **44**, 863 (2020).
- [64] K. Y. Bliokh, A. Y. Bekshaev, A.G. Kofman, and F. Nori, Photon trajectories, anomalous velocities and weak measurements: a classical interpretation, New J. Phys. **15**, 073022 (2013).